11th International Symposium on Magnetic Bearings
August 26-29, Nara, Japan

DEVELOPMENT AND APPLICATION OF PARALLEL PM TYPE HYBRID MAGNETIC BEARINGS

Yohji Okada
Dept. of Mechanical Eng., Ibaraki University, Hitachi, Ibaraki-Pref., 316-8511 Japan
y.okada@mx.ibaraki.ac.jp

Kouji Sagawa
Dept. of Mechanical Eng., Ibaraki University, Hitachi, Ibaraki-Pref., 316-8511 Japan

Eisaku Suzuki
Dept. of Mechanical Eng., Ibaraki University, Hitachi, Ibaraki-Pref., 316-8511 Japan

Ryou Kondo
Dept. of Mechanical Eng., Ibaraki University, Hitachi, Ibaraki-Pref., 316-8511 Japan
rkondo@mx.ibaraki.ac.jp

ABSTRACT
Hybrid magnetic bearing is recognized as an efficient one even with wide airgap and suitable for low loss and wide gap application. Previously sub-pole type IPM hybrid magnetic bearing has been proposed. However the sub-pole produces bias flux and cannot produce any control force. To overcome this problem, two new types of hybrid magnetic bearings are proposed which have permanent magnets within their stator cores. This paper introduces structure and principle of the proposed magnetic bearings. The geometric parameters of these new type magnetic bearings are optimized using FEM analysis. The experimental setups are made based on these analytical results. The fundamental characteristics are measured and compared with the estimated bearing performances. The results show stable levitation and good levitated rotation.

INTRODUCTION
Recently low cost and highly efficient magnetic bearings are requested and developed. Standard magnetic bearings use electro-magnets to produce bearing force. This type has defects of low efficiency and temperature rise when it applies to the wide gap application. On the contrary hybrid (HB) type magnetic bearings are considered to have high efficiency and good linearity because it uses permanent magnets to produce strong bias flux [1] [2]. Especially high force factor of the HB magnetic bearing is important characteristics for applying to the wide air gap rotors. Previously internal permanent magnet (IPM) type magnetic bearing is proposed and reported, as shown schematically in Fig. 1. This magnetic bearing has the bias permanent magnets within the radial magnetic bearing and all the magnetic circuit is closed inside the radial magnetic bearing [3] [4] [5]. Hence this type has the merits of small size and low flux leakage. However, the IPM type magnetic bearing uses main-pole for producing the control force and sub-poles for bias permanent magnet which cannot produce any control force. Hence the maximum control force is considered lower than the standard electro-magnet type AMB. To overcome this problem, two types of parallel PM type magnetic bearings are proposed and reported in this paper. These two types use only the main-poles which can produce the control force and the bias permanent magnets are installed between the main-poles. Both types are designed and fabricated. The test results are reported and compared. Finally the applicability to the wide gap rotor is discussed.

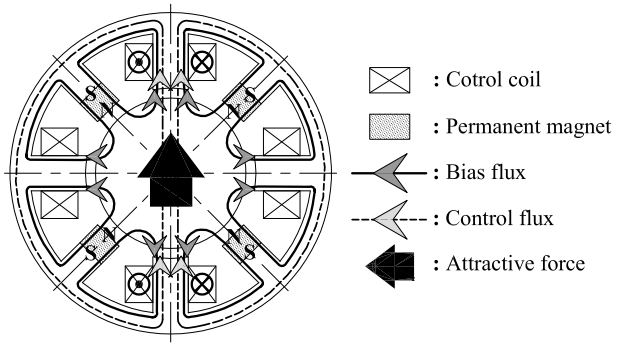

FIGURE 1: Schematic of internal permanent magnet (IPM) type hybrid magnetic bearing

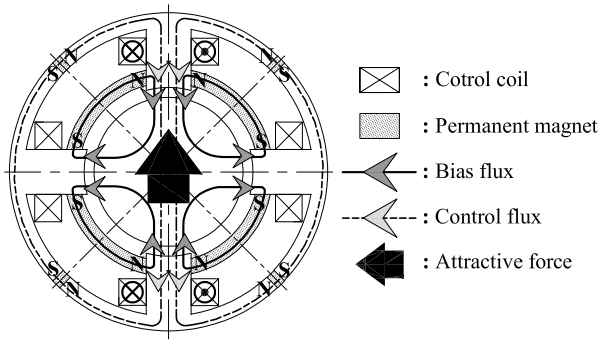

FIGURE 2: Principle of type 1 magnetic bearing

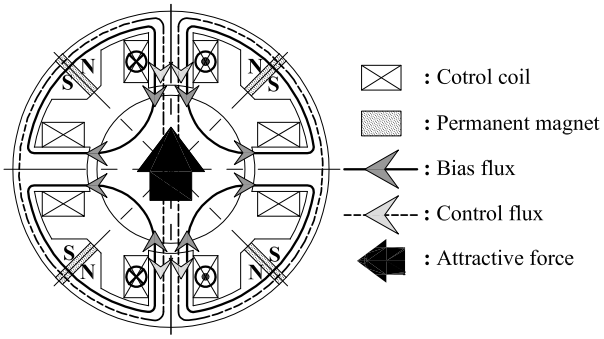

FIGURE 3: Principle of type 2 magnetic bearing

PARALLEL PM TYPE MAGNETC BEARINGS

Schematic of Type 1 magnetic bearing is shown in Fig. 2. This type has the bias permanent magnets between the adjacent bearing poles. The sub-poles are not necessary and all salient poles can produce control force which have the coil windings. The bias flux produced by the PMs are shown by the solid lines in Fig. 2. To avoid the flux leakage into the outer core guide PMs are installed in the middle of the outer core of the stator. This structure can produce enough bias flux between the control pole and the rotor core. We call this type AMB as parallel PM type because the bias permanent magnets are installed parallel to the rotor core. The only defect of this type is considered flux leakage from the outer PMs. Hence the design should be considered to increase the thickness of the stator holder to avoid the flux leakage to the surrounding space.

Fig. 2 illustrates the case when upward control force is produced. The control current is flowed as shown in the figure to produce the control flux shown by the dashed lines. The flux in the upper air gap is increased while that in the lower air gap is decreased. This flux difference produces the attractive force difference which in turn causes the upward control force. The similar control scheme is applied to the left and right control coils. Hence two dimensional radial directions can be controlled.

The operating principle of type 2 magnetic bearing is shown schematically in Fig. 3. Type 2 has the bias PMs only in the outer core of the stator which have wider PM surface. This type has the merit of low parts number and the operating principle is similar to type 1. The bias flux flows from the N pole of PM surface to the stator main pole. Then flux flows into the rotor core and then to the adjacent pole back to the S pole surface of the PM as shown by the solid line in the figure. The permanent magnets have wide surface and thinner thickness which is expected to produce enough flux in the air gap and to have lower reluctance to the control flux. Hence the permanent magnets are extended to the inner space from the outer yoke. The control force is produced similarly by producing the control flux as shown by the dashed line in the figure.

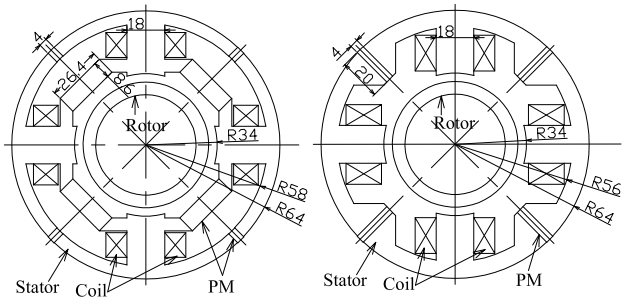

FIGURE 4: Analytical models (Left: Type 1, Right: Type 2)

TABLE 1: Parameters of analytical model

Item	Value (Material)
Air gap	4 [mm]
Magnetic material	Laminated silicon steel
Lamination depth	30.1 [mm]
Coil turns	500 [turns/slot]
Permanent magnet	NEOMAX-39SH

EXPERIMENTAL SETUP

To confirm the proposed two types of IPM magnetic bearings, the experimental setups are designed and fabricated.

Design Using FEM Analysis

To determine detailed size of the radial magnetic bearings, two dimensional magnetic field analysis using ANSYS is carried out. Figure 4 shows analytical model of types 1 and 2 magnetic bearings. They are determined after several analytical iterations. This magnetic bearing is considered to apply to the wide gap canned pump. Hence the air gap between the rotor and stator is determined 4 [mm]. The other pa-

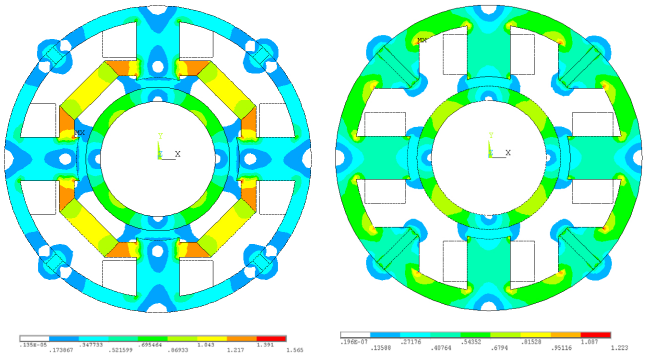

FIGURE 5: Flux density (Left: Type 1, Right: Type 2)

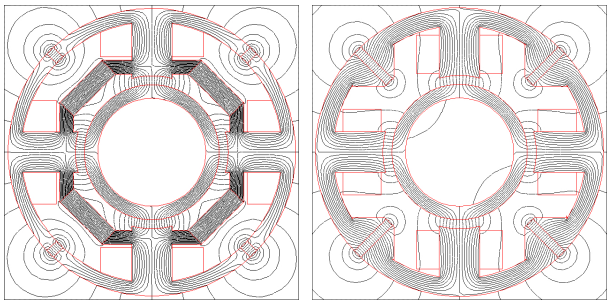

FIGURE 6: Flux lines (Left: Type 1, Right: Type 2)

rameters are determined through the analysis. The main parameters are listed in Table 1. This IPM type HB magnetic bearing can be applicable to the even salient pole number ≥ 4. For practical simplicity 4 pole magnetic bearing is only designed in this paper. The thickness of lamination is determined 30.1 [mm].

The calculated flux density distributions and flux lines are shown in Figs. 5 and 6. Both cases show enough bias flux even 4 [mm] wide air gap. The flux circuit is well formed without any serious saturation. The flux density distribution on the rotor surface is shown by the solid lines in Fig. 7. The flux at the salient pole show N and S poles alternatively because the PMs are installed between the adjacent salient poles. The flux densities at the main pole is 0.32−0.37 [T] for type 1 and 0.31−0.35 [T] for type 2 which are considered enough high flux. The dots in Figs. 7 to 9 are the experimental results mentioned later.

The negative force characteristics are shown by the solid lines in Fig. 8. They are calculated by moving the rotor from the center of stator to one of the pole by 0.1 [mm] step with zero control current. The results of both cases show about 18.9 [N] negative force at 1 [mm] rotor displacements.

Similarly the control forces are calculated as shown by the solid lines in Fig. 9. In this case the rotor is fixed in the center of the stator and the control current is increased by 0.1 [A] step which flows series connected coils of the opposite pole. The control forces are about 24.5 [N] for type 1 and 28.7 [N] for type 2 at 1 [A] control current. Thanks to the strong bias flux and wide air gap the linearity is very good. The control force is enough and can levitate the rotor easily with considering the previously calculated negative force characteristics.

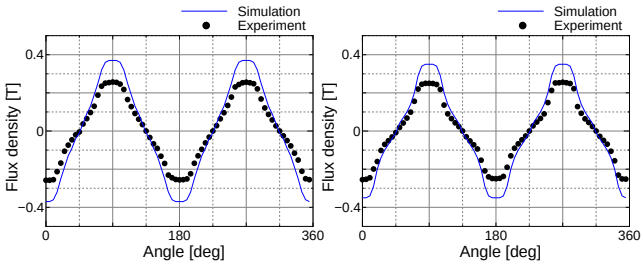

FIGURE 7: Flux density distribution (Left: Type1, Right: Type2)

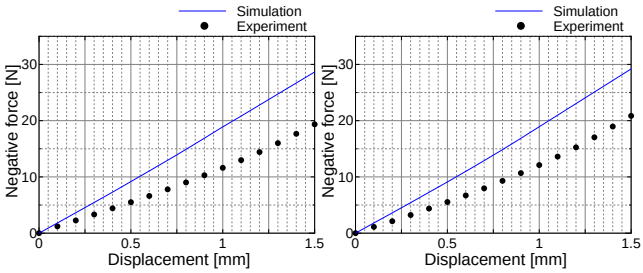

FIGURE 8: Negative force (Left: Type1, Right: Type2)

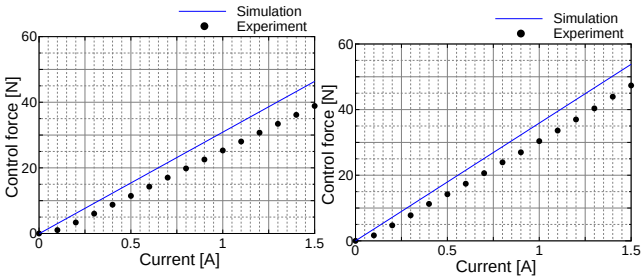

FIGURE 9: Control force (Left: Type1, Right: Type2)

Design of the stator

The stator parts are shown in Fig. 10 for type 1 and in Fig. 11 for type 2, respectively. They are made individually and assembled with 4 core parts and permanent magnets. The assembling parts number of type 2 is less than that of type 1. After assembled the out diameter is 128 mm and the thickness is 30.1 mm. The cores are laminated with 0.35 [mm] silicon steel and the bias permanent magnet used is NEOMAX-39SH.

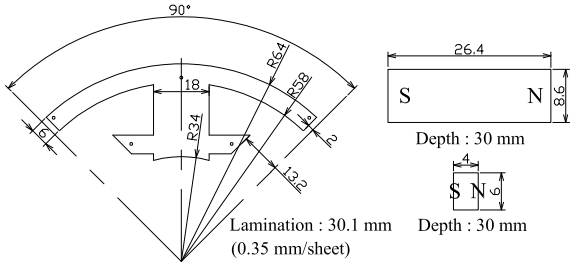

FIGURE 10: Schematic of type 1 stator (Left: Stator core, Right: Permanent magnet)

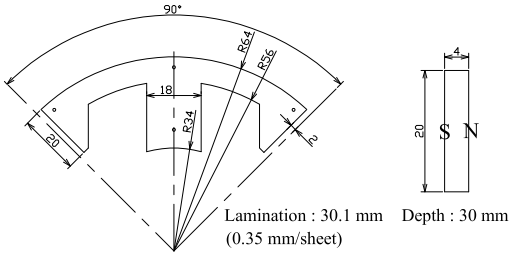

FIGURE 11: Schematic of type 2 stator (Left: Stator core, Right: Permanent magnet)

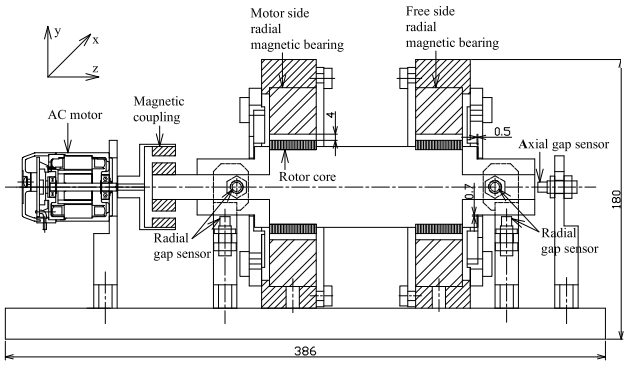

FIGURE 12: Schematic of experimental setup (side view)

Assembled Experimental Setup

The side view and front view of the experimental setup are shown in Figs. 12 and 13, respectively. The rotor is supported by two radial magnetic bearings in horizontal position. The axial direction relies on passive stability and is not controlled actively. The rotor is commonly used for stator types 1 and 2. The rotor weight is 1.519 [kg]. As mentioned the air gap is 4 mm. For practical canned pump application the rotor and stator should be covered by plastic for sealing. Hence the movable area is limited to $\pm$ 0.7 [mm] by touch down. The experiments are carried out similarly by giving the rotation with AC motor through magnetic coupling. Two stators are named; one is motor side which is near motor and the other is free side.

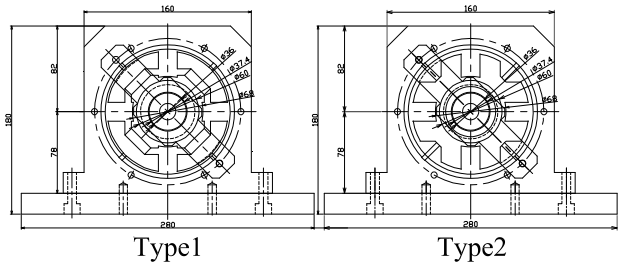

FIGURE 13: Schematic of experimental setup (front view)

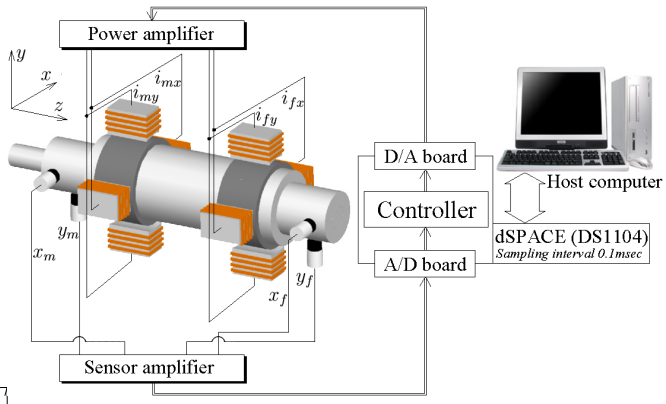

FIGURE 14: Control system

Control System

Scheme of the control system is shown in Fig. 14. The rotor displacements are measured by eddy current type gap sensors. These four x, y displacement signals are put into DSP (dSPACE DS1104) via A/D converters. After calculating the actuating signals they are put out to power amplifiers (PA12, magnification of -1 [A/V] and supply voltage of $\pm$ 24 [V]) via D/A converters.

The upper and lower coils are connected series to control y direction and the right and left coils are connected series to control x direction, respectively. The control system used is the local PID controller, the gains of which are determined experimentally as shown in Table 2. The sampling interval used is 0.1 [msec], and the derivative time constant is 0.8 [msec].

EXPERIMENTAL RESULTS

Static Characteristics

First, the static characteristics are measured with the assembled rotor and stator pair for type 1 and type 2 magnetic bearings. The flux density distributions, the negative forces and the control forces are shown by the dots in Fig. 7, Fig. 8 and Fig. 9, respectively. The maximum flux density is about 0.257 [T] for type 1 and 0.256 [T] for type 2, which are about

TABLE 2: PID control gains

Type 1					
Item	Motor side value		Free side value		Unit
	y-dir.	x-dir.	y-dir.	x-dir.	
K_P	2500	2000	2500	2000	[A/mm]
K_D	10	8	10	10	[A·sec/mm]
K_I	10000	10000	10000	10000	[A/sec·mm]

Type 2					
Item	Motor side value		Free side value		Unit
	y-dir.	x-dir.	y-dir.	x-dir.	
K_P	2500	2000	2500	2000	[A/mm]
K_D	10	7	10	10	[A·sec/mm]
K_I	10000	10000	10000	10000	[A/sec·mm]

TABLE 3: Static characteristics (Experiments)

	Type 1	Type 2
Max. flux density	0.257 [T]	0.256 [T]
Negative stiffness	11.6 [kN/m]	11.9 [kN/m]
Control force factor	25.3 [N/A]	30.4 [N/A]

70 % of the analytical results. The main reason for the lower experimental flux density is considered due to the three dimensional flux leakage which is not considered in the two dimensional analysis. However, the maximum flux is relatively high compared with the large air gap of 4 [mm].

Next, the negative forces and control forces are measured as shown by the dots in Figs. 8 and 9, respectively. The type 1 control force factor is 25.3 [N/A] and the negative force factor is 11.6 [kN/m], while the type 2 control factor is 30.4 [N/A] and the negative force factor is 11.9 [kN/m], respectively. The negative force factor is about 60 %, while the control force factor is about 80 % compared with the analytical values. They are listed in Table 3 and considered enough strong for controlling magnetic bearings.

Dynamic Characteristics

To confirm the levitation stability the frequency responses are measured and recorded as shown in Figs. 15 and 16, respectively. The rotor is levitated stably with the dSPACE based PID controller. Then the sinusoidal signal of $\pm$ 0.05 [mm] vibration is added to the sensor position in the controller and the corresponding vibration responses are measured. The graphs indicate the responses of motor side. The peaks near 50 [Hz] are well reduced both for type 1 (Fig. 15) and type 2 (Fig. 16). From these results the peak with unbalance response is considered near 3000 [rpm].

The impulse response tests are carried out and

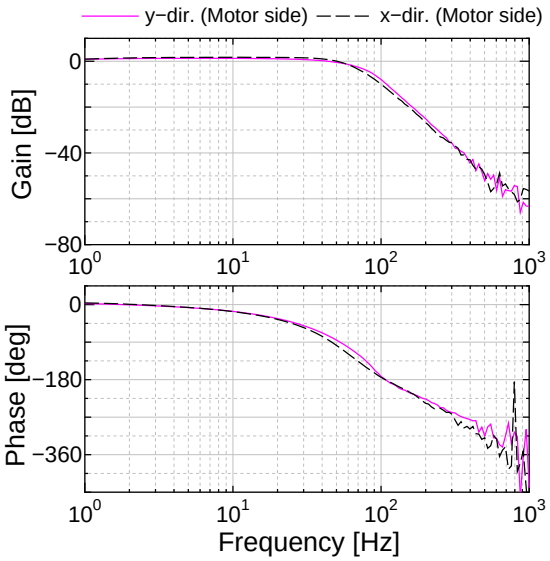

FIGURE 15: Frequency response (Type 1, Motor side)

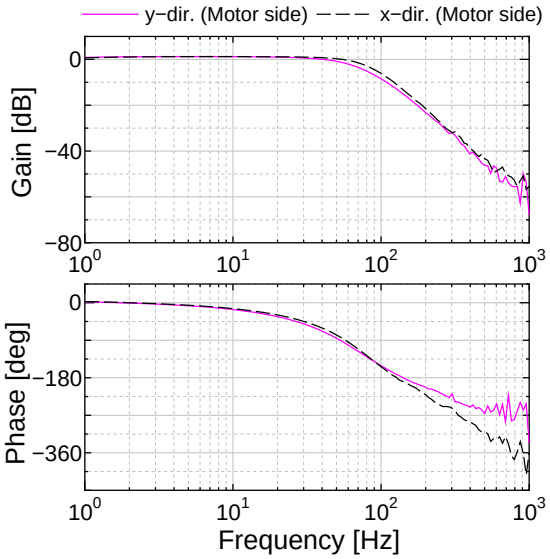

FIGURE 16: Frequency response (Type 2, Motor side)

the results are shown in Figs. 17 and 18, respectively. The y direction of the motor side is hammered to produce about 0.2 [mm] displacement when the rotor is levitated stably. The decaying transient responses are measured as shown in the figures. The vibration has decayed about 0.02 [sec] after hammering for both type 1 and 2. Also the coupled vibration between x and y directions are not recognized. Hence we can conclude that the levitation is very stable.

Levitated Rotating Test

The levitated rotating tests are carried out and the unbalance responses are measured as shown in Figs. 19 and 20, respectively. The rotor is levitated stably

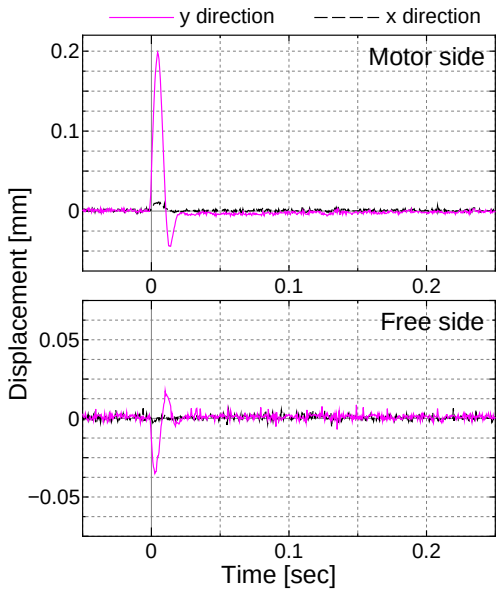

FIGURE 17: Impulse response (Type 1, Motor side, y-direction)

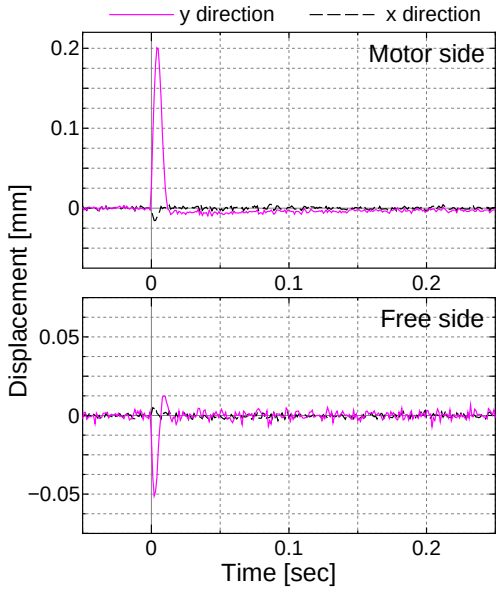

FIGURE 18: Impulse response (Type 2, Motor side, y-direction)

and the rotation is increased by the motor with 200 [rpm] step. After the rotating speed reaches steady state the vibration magnitude is recorded. However the axial direction has sharp peak hence the unbalance is measured with small rotation speed step near peak.

From the measured results the radial vibration increases with the increase of the rotating speed. The vibration of free side is slightly bigger than the motor side. This is considered that the motor side is connected to magnetic coupling which affects adversely to free side results. The vibration of type 2 is slightly

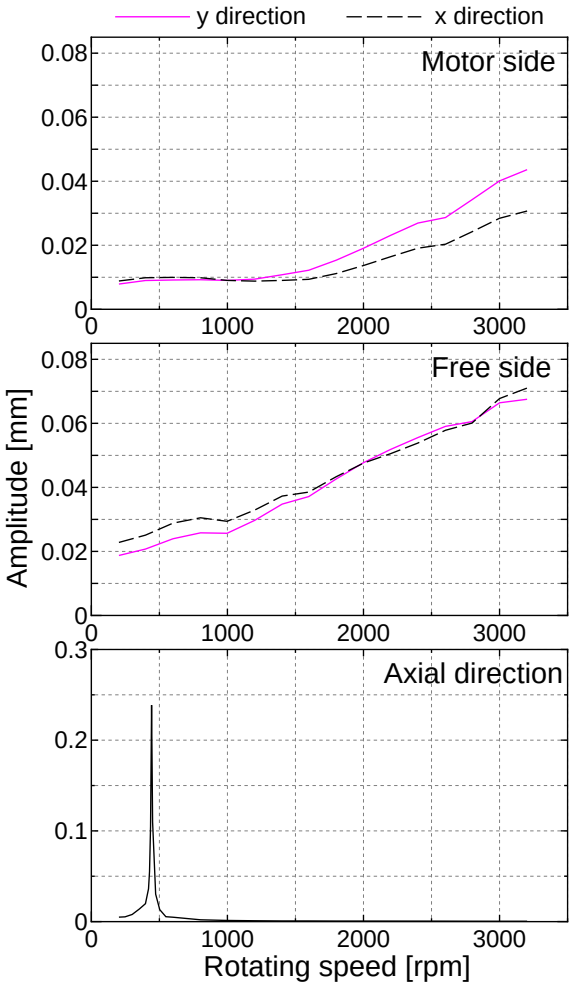

FIGURE 19: Unbalance response (Type 1)

lower than that of type 1. Both radial vibrations, however, are lower than 0.08 [mm] and the rotation is very stable. Top speed is limited up to 3300 [rpm] which is the limit of driving motor speed. Hence we can easily increase the top speed by redesign.

The axial vibration peaks are about 400 [rpm] and the maximum vibrations reach to 0.23 [mm] for type 1 and 0.07 [mm] for type 2. However we can increase the rotor speed with only passive stability. Above the resonant speed the axial vibration is low and stable.

Thanks to very stable and strong bearing control the power consumption of the magnetic bearing is slightly over 1 [W].

CONCLUDING REMARKS

Two types of internal permanent magnet type HB magnetic bearings are proposed in this paper which does not require any sub poles. All the salient poles can produce attractive force which are considered

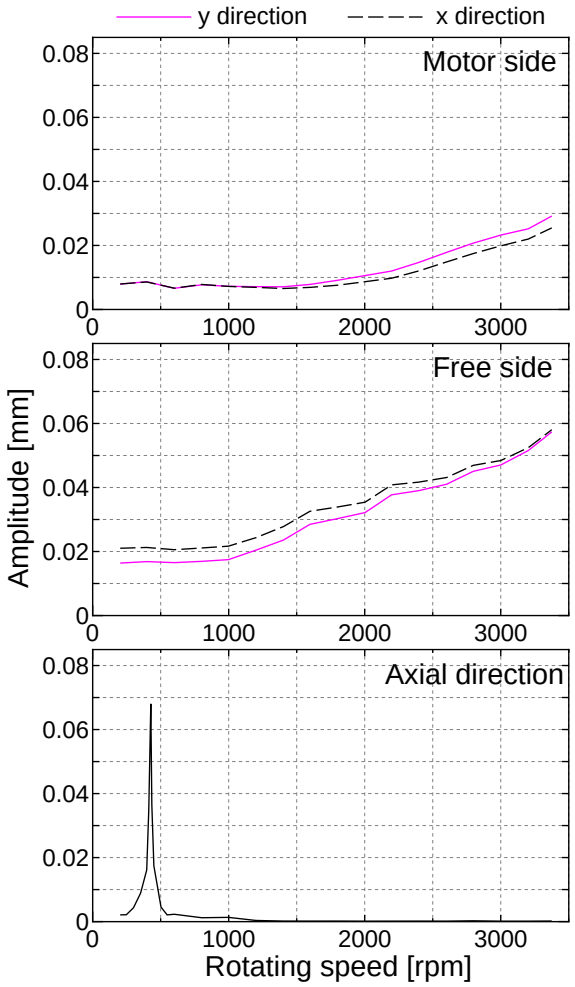

FIGURE 20: Unbalance response (Type 2)

stronger than the previous IPM type magnetic bearings.

Both types are designed using FEM magnetic analysis and the experimental setups are fabricated. Their control force factors indicate about 25.3 [N/A] for type 1 and about 30.4 [N/A] for type 2. They show very strong control force and good levitation properties.

The rotor can run up to 3300 [rpm] which is the driving motor speed limit. The maximum vibration is less than 0.08 [mm]. Axial direction relies on the passive stability, but the rotor can run above the axial resonant peak and does not cause any trouble.

From these experimental results the proposed magnetic bearing is very useful, especially for wide gap applications. Future research work includes to develop the axial magnetic bearing for wide gap applications.

ACKNOWLEDGEMENT

This work is cooperated with Oita Prefecture Collaboration of Regional Entities for Advancement of Technology Excellence, JST.

References

1. Okada, Y., et. al, *Fundamentals and Application of Magnetic Bearings*, (1995), pp. 1-187, JSME New Technology Series No. 1, Yokendo Co., Ltd. (in Japanese)

2. Schweitzer, G., Bleuler, H. and Traxler, A., *Active Magnetic Bearings*, Hochschulverlag AG an der ETH Zurich, 1994.

3. Kakihara, K., Koyanagi H., Okada Y., Development of Built-in PM Type Hybrid Magnetic Bearing, *Transaction of the Japan Society of Mechanical Engineers, Series C*, Vol. 71, No. 710 (2005), pp.2968–2974, (in Japanese)

4. Okada Y., Koyanagi H., Kakihara, K., MiracBearings: New Concept of Miracle Magnetic Bearings, *CD-ROM, Proc. of Ninth Int. Symp. of Magnetic Bearing*, August, 3-6, (2004), Lexington, Kentucky, USA, pp. 1-6

5. Reisinger, M., Amrhein W., Silber, S., and Peter, R., Development of a Low Cost Permanent Magnet Biased Bearing, *CD-ROM, Proc. of Ninth Int. Symp. of Magnetic Bearing*, August, 3-6, (2004), Lexington, Kentucky, USA, pp. 1-6